



OPEN

Performance comparison of Gilbert's algorithm and machine learning in classifying Bell-diagonal two-qutrit entanglement

Marcin Wieśniak

While classifying states as entangled or separable is one of the fundamental tasks in quantum information theory, it is also extremely challenging. This task is highly nontrivial even for relatively simple cases, such as two-qutrit Bell-diagonal states, i.e., mixtures of nine mutually orthogonal maximally entangled states. In this article we apply Gilbert's algorithm to revise previously obtained results for this class. In particular we use "entanglement cartography" to argue that most states left in [Hiesmayr, B. C. *Scientific Reports* 11, 19739 (2021)] as unknown to be entangled or separable are most likely indeed separable, or very weakly entangled, beyond any practical relevance. The presented technique can find endless applications in more general cases.

Entanglement is probably the most striking feature of quantum mechanics. Initially, it was introduced for pure states, as a notion that parts of a composite quantum system can be described only in reference to each other¹. This understanding was extremely convenient, as it was immediate to recognize an entangled state, and as it turned out², in the bipartite case, entanglement can be quantified uniquely as the entropy of reduced states of subsystems.

However, as the interest in foundations of quantum information theory grew, the issue got more complicated. For mixed quantum states, mathematically represented by positive semi-definite square matrices of trace 1, it is not sufficient to study the deficit of information about individual subsystems at the expense of correlations. Instead, one needs to consider if the correlations can be reconstructed by means of local operations and classical communication (LOCC). A strong indicator of presence of entanglement in a state is a negative partial transpose (NPT)^{3,4}. Still, it turned out that, except for dimensions of subsystems 2×2 and 2×3 , entangled states with positive partial transpose (PPT) exist⁵. This form of entanglement has been recognized as bound entanglement, which cannot be distilled to the form of maximally entangled states⁶, as opposed to free NPT entanglement. Technically, it remains an open question if bound entangled states with a negative partial transpose exists, but hereafter we will assume that all NPT entanglement is distillable.

More generally, all positive, but not completely positive maps were found to identify some form of entanglement⁴. Alternatively, any entangled state yields a negative mean value of a suitable entanglement witness operator, for which all separable (non-entangled) states give non-negative means (hereafter, we will adapt the opposite convention). The two methods happen to be related to each other by the Jamiołkowski-Choi isomorphism^{7,8}. However, until recently there were no practical means to construct a witness tailored for a given state.

Further complications arose with attempts to give reasonable measures of entanglement. A list of requirements that any such measure must satisfy was formulated⁹ and two operational measures were defined: distillable entanglement⁹ and entanglement cost¹⁰. The former quantifies the number of Bell states required to prepare a copy of a given state in the LOCC, while the latter gives the number of them in the opposite process. Other measures were proposed in hope for better computability, for example based on the notion of a closest separable state (CSS)¹¹, or as extensions of the measure for pure states with a convex roof extension¹². Still, the impossibility of considering all possible state manipulation schemes, decompositions into pure states and apparent computational difficulty of computing CSS with respect to some metrics prevented all of these propositions to become universal and practical.

¹Faculty of Mathematics, Physics, and Informatics, Institute of Theoretical Physics and Astrophysics, University of Gdańsk, 80-308 Gdańsk, Poland. ²International Centre for Theory of Quantum Technologies, University of Gdańsk, ul. Bażyńskiego 1A, 80-309 Gdańsk, Poland. email: marcin.wiesniak@ug.edu.pl

More modern computing techniques have also been employed to the problem of separability in specific cases. For example, there was a number of attempts to adopt machine learning techniques to distinguish entangled states from separable ones^{13–25}. This approach poses its own set of challenges. First, as every use of machine learning (ML) techniques is application-specific, relatively little can be said about, e.g., the optimality of the topology of a neural network, the form of the activation function, etc.. The other issue is that the result of ML is dependent on the training data, which can be very limited for the entanglement-vs-separability problem. An algorithm can become overtrained, with a fixation on the presented pattern. Finally, neural networks are not designed to estimate the missing continuous value of a function, which makes them less capable of providing the interpolation of the amount of entanglement, although there were some attempts of such tasks^{20,21}.

Recently, other strategies for classifying states as entangled or separable, based on variational algorithms²⁶ and semi-definite programming²⁷, were proposed.

In this article we compare the algorithmic approach described in detail below with ML results obtained by Hiesmayr¹⁷, who focused on “the magic simplex”, or the set of Bell-diagonal states of three qubits. The task is to classify states as free entangled, bound entangled, or separable. Our methodology is described below, followed by a presentation of results and conclusions.

Hilbert-Schmidt distance and Gilbert’s algorithm

The Hilbert-Schmidt distance between arbitrary matrices A and B of the same size is defined simply as

$$\begin{aligned} D_{HS}(A, B) &= \sqrt{\text{Tr}((A - B)(A - B)^\dagger)} \\ &= \sqrt{\sum_{j,k} |(A - B)_{j,k}|^2}, \end{aligned} \quad (1)$$

with $\text{Tr}(\cdot)$ denoting the trace and $(X)_{j,k}$ denotes the element at the position (j, k) of the matrix X .

This figure of merit has many advantages. Obviously, it is a well-defined distance, being just a variant of the usual Euclidean metric. It also allows us to use intuitive terms from everyday geometry, such as spheres, angles, or intervals. It is also the only measure, which can be calculated without a computationally expensive subroutine for singular decomposition of a matrix.

Unsurprisingly, it was suggested as a core of an entanglement measure by Witte and Trucks²⁸. For state ρ this entanglement quantifier shall be defined as

$$D_{HS}(\rho) = \min_{\sigma \in SEP} D_{HS}(\rho, \sigma), \quad (2)$$

where the minimum is taken over all separable states. However, it was shown by Ozawa²⁹ that the Hilbert-Schmidt distance does not comply with the requirement of contractivity under a local operation applied to both states, although it remains unclear if it holds for the minimalization. Other complications may occur when migrating a state to another Hilbert space by adding or tracing out an auxiliary system. Still, given the advantages of the Hilbert-Schmidt measure, it can be seen as an insightful quantifier of non-classical correlations.

In 1966, Gilbert³⁰ introduced an algorithm to estimate the distance between a given point and a convex set. It was demonstrated to be useful to show the membership of a state in an LOCC equivalence class³¹, and to optimize Bell operators³². Finally, Pandya, Sakarya, and Wieśniak³³ discussed a direct use of the algorithm to estimate the distance of a given quantum state to the set of separable states. The algorithm can be outlined as follows.

Algorithm 1 (bipartite case):

Input: test state ρ_0 , initial separable state ρ_1 .

Output: approximation of CSS ρ_1 , list of squared distances to subsequent CSS approximations l .

1. Take random pure state $\rho_2 = |\varphi_A\rangle|\varphi_B\rangle\langle\varphi_A|\langle\varphi_B|$, that will be referred to as a trial state (run Algorithm 2).
2. If the preselection criterion, $\text{Tr}(\rho_0 - \rho_1)(\rho_2 - \rho_1) > 0$ is not met, go to step 1 or abort if the HALT condition is satisfied.
3. Maximize $\text{Tr}(\rho_0 - \rho_1)(\rho_2 - \rho_1)$ with local unitary transformations (run Algorithm 3).
4. Update $\rho_1 \leftarrow p\rho_1 + (1 - p)\rho_2$ for p minimizing $D_{HS}(\rho_0, p\rho_1 + (1 - p)\rho_2)$.
5. Every 50 corrections append $D_{HS}^2(\rho_0, \rho_1)$ to l .
6. If the HALT condition is not met, go to step 1, otherwise quit.

Pure random states are generated in the following subroutine³⁴.

Algorithm 2 :

Input: dimension d .

Output: pure d -dimensional state randomly generated with respect to the Haar measure $|\psi\rangle$.

1. Draw $2d$ random numbers r_1, r_2, \dots, r_{2d} from a normal distribution centered at 0.
2. Construct $|\psi\rangle = \{c_j\}_{j=1}^d = \{r_{2j-1} + ir_{2j}\}_{j=1}^d$.
3. Normalize $|\psi\rangle$ so that $\langle\psi|\psi\rangle = 1$.

Hereafter, i will denote the imaginary unit, $i^2 = -1$.

Features and performance of Algorithm 1 have been studied in Ref.³³, with two major updates introduced in this work. One of them is the optimization in Step 3, which, depending on ρ_0 , can speed up the convergence up to approximately 50 times, in terms of the required number of trials. In the code used for this article the optimization was performed with the following algorithm.

Algorithm 3 :

Input: states ρ_0, ρ_1 and ρ_2 .

Output: optimized state ρ_2 .

For $j = 1$ to 1500:

do

1. draw a pure random qutrit state $|\psi\rangle$ uniformly with respect to the Haar measure (run Algorithm 2).
2. With j odd construct

$$U = (\mathbb{1} + (e^{i\pi/100} - 1)|\psi\rangle\langle\psi|) \otimes \mathbb{1}. \tag{3}$$

With j even construct

$$U = \mathbb{1} \otimes (\mathbb{1} + (e^{i\pi/100} - 1)|\psi\rangle\langle\psi|). \tag{4}$$

3. If $\text{Tr}(\rho_0 - \rho_1)(\rho_2 - \rho_1) > \text{Tr}(\rho_0 - \rho_1)(U\rho_2U^\dagger - \rho_1)$, replace $U \leftarrow U^\dagger$
4. replace $\rho_2 \leftarrow U\rho_2U^\dagger$ until $\text{Tr}(\rho_0 - \rho_1)(\rho_2 - \rho_1) > \text{Tr}(\rho_0 - \rho_1)(U\rho_2U^\dagger - \rho_1)$

done.

The algorithm provides three pieces of information that can be used here to classify states as entangled or separable. The first is, rather trivially, the last squared distance D_{Last}^2 found within a fixed number of corrections. For systems of this size, the distance obtained after more than 1000 corrections is believed to be a fairly good representation of the actual distance. In fact, some separable states can be reconstructed nearly down to the numerical precision in a few corrections, and are therefore safely assumed to be separable. As the algorithm in principle cannot reach $D_{\text{Last}}^2 = 0$, this indicator tends to overestimate entanglement for states close the entangled-separable boundary. Our approach puts the emphasis on the quantitative, rather than qualitative description of entanglement.

The second indicator is the distance decay estimate, D_{Est}^2 . This is the other improvement with respect to Ref.³³. The current recommendation is to maximize the linear regression coefficient,

$$R(x, y) = \frac{\text{Cov}(x, y)}{\sqrt{\text{Var}(x)\text{Var}(y)}}, \tag{5}$$

with Cov and Var denoting covariance between the list of correction numbers c and $1/(l - a)$ (each element of l is shifted by a and then inverted), and the variances of these lists. We reject the first one third of the entries, after which the lists are denoted by $\tilde{\cdot}$. We thus have

$$D_{\text{Est}}^2 = \text{argmax}_a R(\tilde{c}, 1/(\tilde{l} - a)), 0 \leq a \leq \min l. \tag{6}$$

Here, $\text{argmax}_x f(x)$ yields the value of x that maximizes $f(x)$. Although, unlike the other two indicators, D_{Est}^2 does not certify anything, but is merely an result of a statistical analysis, we shall find it to be quite informative. With $R(x, ex + f) = 1, e > 0$ and f being real numbers, we typically get $R \approx 0.998$ for 10,000 corrections.

One advantage of D_{Est} over D_{Last} is that the distance decay estimate can be found to be 0, suggesting no entanglement in the studied state.

The third and final figure of merit considered here is the witness distance estimate D_{Wit} . As Ref.³⁵ points out, if $\rho_{0,\text{CSS}}$ is the actual closest separable state, operator $W_0 = \rho_0 - \rho_{0,\text{CSS}}$ attains positive expectation values only for entangled states, thus being an entanglement witness. In reality, ρ_1 is only an approximation of $\rho_{0,\text{CSS}}$, displacing and tilting the hyperplane represented by the witness. As stated in Ref.³⁶, we then need to consider

$$W = \rho_0 - \rho_1 - \mathbb{1} \max_{|\phi_1\rangle, |\phi_2\rangle} \langle\phi_1|\langle\phi_2|(\rho_0 - \rho_1)|\phi_1\rangle|\phi_2\rangle, \tag{7}$$

with the maximum taken over all product states. Then

$$D_{\text{Wit}} = \max \left(0, \frac{\text{Tr}W\rho_0}{\sqrt{\text{Tr}(\rho_0 - \rho_1)^2}} \right). \tag{8}$$

Again, this quantity depends on the quality of the approximation ρ_1 , and provides a bound, this time lower, on the actual distance. It is the only one, out of the three quantities, that actually certifies the presence of entanglement. However, calculating it is more challenging computationally than it seems. To claim to have found the global maximum of a trigonometric polynomial we need to have a high confidence level that we did not obtain a value for any local extrema. This is done, for example, by multiple repetitions of the maximization with randomized initial conditions. Having taken care of it, we shall assume that we have indeed found the absolute maximum.

“Magic Simplex” states

Equipped with the above tools to analyse entanglement, we will revisit certain classes of two-qutrit Bell diagonal states, also known as “Magic Simplex” states.

Let us consider a maximally entangled state of two qutrits,

$$|\psi_{00}\rangle = \frac{1}{\sqrt{3}} \sum_{j=0}^2 |jj\rangle, \quad (9)$$

and two Weyl operators, $X = \begin{pmatrix} 0 & 1 & 0 \\ 0 & 0 & 1 \\ 1 & 0 & 0 \end{pmatrix}$ and $Z = \begin{pmatrix} 1 & 0 & 0 \\ 0 & \alpha & 0 \\ 0 & 0 & \alpha^2 \end{pmatrix}$ with $\alpha = e^{2i\pi/3}$. The Bell basis is given by

$$\{|\psi_{jk}\rangle\}_{j,k=0}^2 = \left\{ \mathbb{1} \otimes X^j Z^k |\psi_{00}\rangle \right\}_{j,k=0}^2. \quad (10)$$

Then the Bell-diagonal states are

$$\rho = \sum_{j,k=0}^2 p_{jk} |\psi_{jk}\rangle \langle \psi_{jk}|, \quad (11)$$

$$\sum_{j,k=0}^2 p_{jk} = 1, p_{jk} \geq 0.$$

In particular, Hiesmayr focused on four families of states. Family *A* was given by

$$\rho(\alpha, \beta, \gamma) = (1 - \alpha - \beta - \gamma) \frac{\mathbb{1}}{9} + \alpha |\psi_{00}\rangle \langle \psi_{00}| + \beta |\psi_{01}\rangle \langle \psi_{01}| + \gamma |\psi_{02}\rangle \langle \psi_{02}|, \quad (12)$$

and it was considered for $\gamma = 0$. The other three families are a part of Family *B*, which includes all the states in form

$$\rho(\alpha, \beta, \gamma, \delta) = (1 - \alpha - \beta - \gamma - \delta) \frac{\mathbb{1}}{9} + \alpha |\psi_{00}\rangle \langle \psi_{00}| + \frac{\beta}{2} (|\psi_{01}\rangle \langle \psi_{01}| + |\psi_{02}\rangle \langle \psi_{02}|) + \frac{\gamma}{3} \sum_{j=0}^2 |\psi_{1j}\rangle \langle \psi_{1j}| + \frac{\delta}{3} \sum_{j=0}^2 |\psi_{2j}\rangle \langle \psi_{2j}|. \quad (13)$$

This family was studied in three different cases. Family B_1 had $\gamma = -\frac{1}{\sqrt{3}}$ and $\delta = 0$, Family B_2 is parameterized by $\gamma = -0.83$ and $\delta = 0$, while B_3 consisted of states with $\alpha = \frac{5}{3}(\sqrt{3} - 1)$ and $\beta = -\frac{1}{10}$.

The aim of this work is to recover, or possibly expand on results presented recently by Hiesmayr in Ref.¹⁷ and to verify the prediction of the machine learning presented therein. For selected families, first, the states were checked for negative partial transposition identifying all the states containing free entanglement (FREE). For the rest, which could be either bound entangled (BOUND) or separable (SEP), other known criteria of entanglement were collected. Another portion of states was recognized as bound entangled in a numerical search of respective entanglement witnesses, reportedly being the most computationally demanding part. Finally, neural networks were trained to classify remaining unknown (UNKNOWN) states as SEP or BOUND. This, however, required pre-assigning a class to each state, to be changed later by the classification algorithms.

These results were later improved to a classification of all Bell-diagonal two-qutrit states³⁷ with probability of about 95%. However, Ref.³⁷ only provides volumetric estimates of entanglement, while Gilbert's algorithm gives more information on the distance.

Results

In this work we utilize a technique of entanglement cartography. For randomly scattered states within a given set, we calculate D_{Last} , D_{Est} , and D_{Wit} . The found values are then interpolated, and the resulting charts can be compared with plots in Ref.¹⁷. The charts contain evidence, if not solid proofs, for the boundaries of BOUND and SEP regions.

Family A

We first focus on Family A, in which we studied 1485 PPT states, each with up to 4000 corrections (the algorithm HALTS at $D_{HS}^2(\rho_0, \rho_1) < 10^{-7}$). Figure 1 presents a 3D plot of D_{Est} . It presents an almost hollow structure. This is due to the plot renderer omitting the extreme values for clarity and the convergence being slower at the boundary between separable and entangled states. The only prominent maxima correspond to small sets bound entangled states confirmed in Refs.^{38,39}. No entanglement witnesses were found. It is thus reasonable to assume that for this family bound entanglement exists only in neighbourhoods found in Refs.^{38,39}.

Close-up

We have thus performed a more detailed study of 160 Family A PPT states with $\alpha \in (0.175, 0.225)$, $\beta \in (-0.075, -0.025)$, and $\gamma = 0$. We started with 90,000 corrections for each state, and extended the study for six states, which had $D_{Est} > 0$. However, within HALT condition of up to 220000 corrections or 2 billion trial states we have found only three states with $D_{Wit}^2 > 0$. We thus leave the issue of the remaining three states unresolved by our method. Nevertheless, we remark that the plot for D_{Est} reproduces the shape of the set of bound entangled states presented in Figure 3 of Ref.¹⁷. It should be also noted that for the eight states with $D_{Est} > 0$ the regression coefficient was greater than 0.9999. The results for D_{Last} , D_{Est} , D_{Wit} are presented in Fig. 2.

Family B

Subsequently, we have conducted the analysis for the remaining three families. Within each family we generated 300 states. For Family B_1 , B_2 , and B_3 we conducted up to 10,000, 8000 and 10,000 corrections respectively. The results are presented in Fig. 3 and they seem to adequately reproduce the plots in Ref.¹⁷. Optimization for states belonging to Family B_2 was significantly slower, meaning that they require significantly more trial states for a correction. Hence, the algorithm was HALTed with fewer corrections.

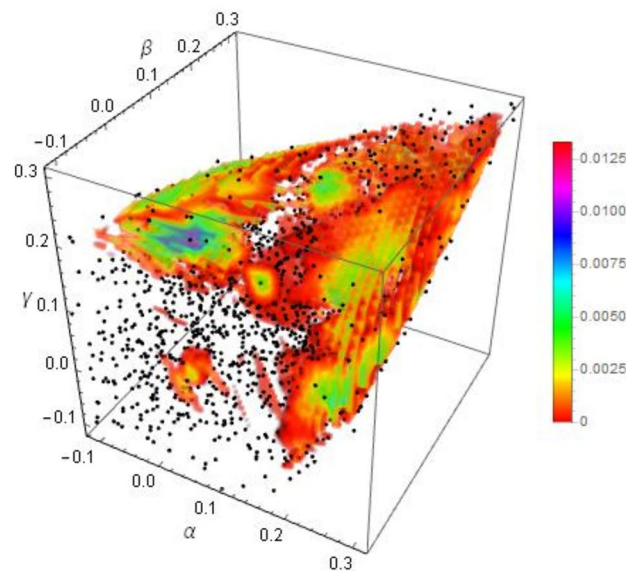


Figure 1. 3D plot of D_{Last} for PPT states from family A. Black dots represent studied states.

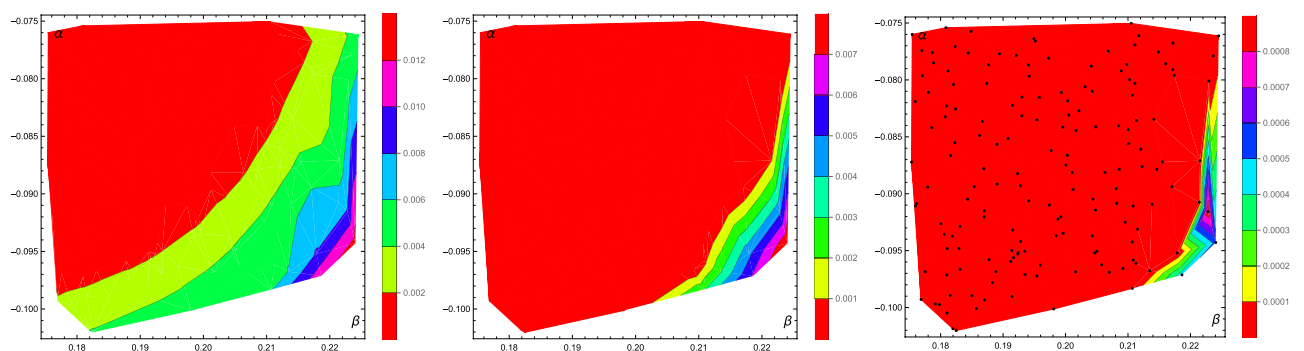


Figure 2. The interpolated plots of D_{Last} (left), D_{Est} (center), and D_{Wit} (right) for Family A with $\gamma = 0$ (only a region with PPT entangled state). Black dots represent studied states.

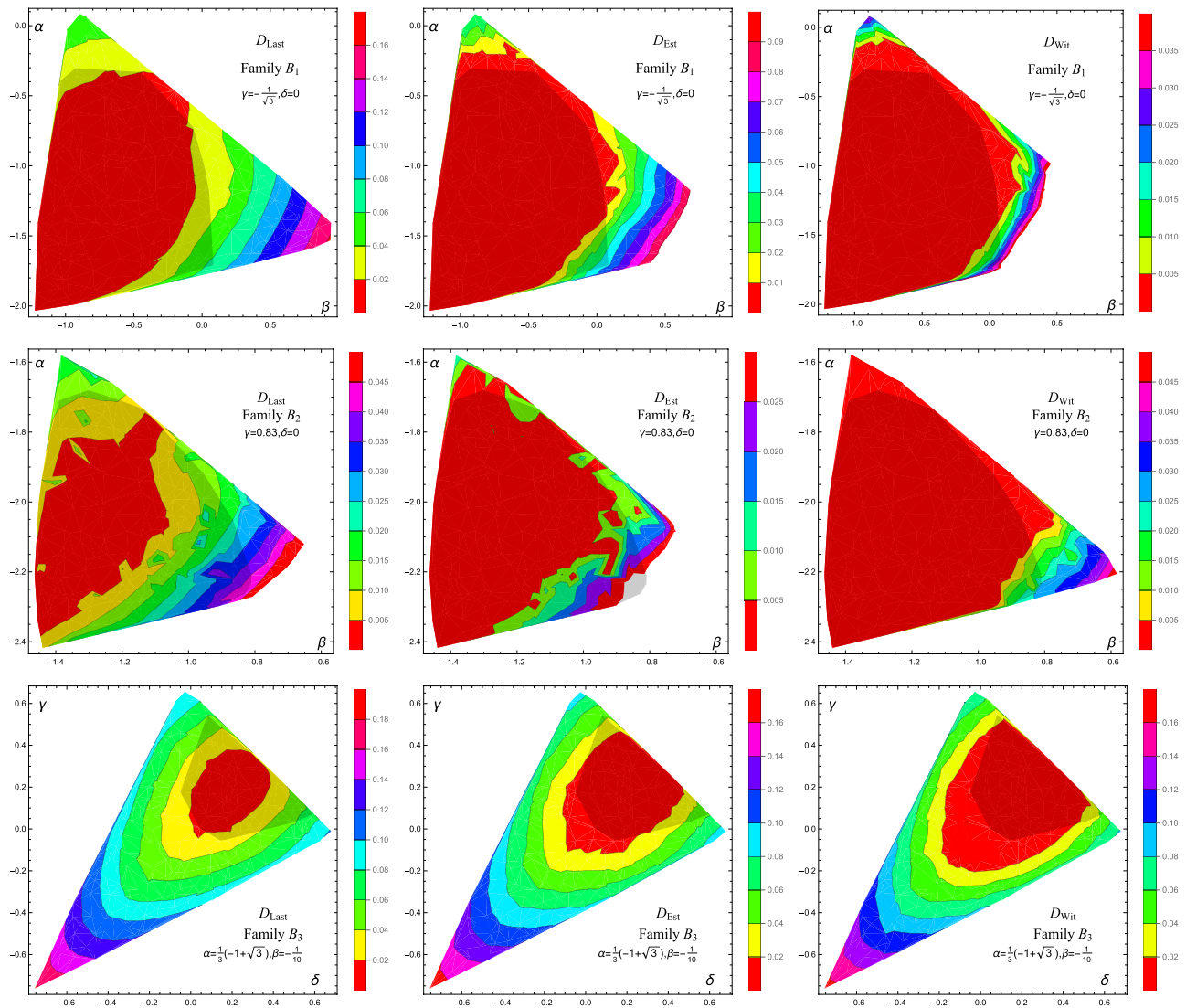


Figure 3. The interpolated plots of D_{Last} (left), D_{Est} (center), and D_{Wit} (right) for Families B_1 (top), B_2 (middle) and B_3 (bottom). Shaded areas represent PPT states.

Close-up of Family B_3

However, we have performed an extensive study of the PPT part of Family B_3 . This Family was chosen primarily because only for families B_2 and B_3 Hiesmayr presented machine learning results with two different preassignment strategies, “random forest” and “nearest neighbours”. For Family B_2 , one of the results suggests all states to be entangled, and both results contradict our findings. For Family B_3 the two approaches gave rather inconsistent results, which are aggregated in Fig. 4. We have generated 160 states, which were studied up to 60,000 corrections each. This number of corrections provided very high consistency between D_{Last} , D_{Est} , and D_{Wit} . We found 32 entanglement witnesses. The results are presented Fig. 5. Importantly, the set of states recognized as entangled exceed the set bounded by witnesses presented in Ref.¹⁷. In this case, the algorithm found a new set of bound entangled states. For example, a state with coordinates $(\gamma, \delta) = (-0.0226, 0.3067)$ was confirmed to be entangled while it was not detected in the original Reference. Also, the boundary between bound entangled and separable states seems to be curved, rather than straight. Given the geometric interpretation of the problem, this is actually expected.

Finer study of Family B_2

We also selected 34 states from Family B_2 that are close to an expected boundary between separable and entangled states. We carried the calculation up to 40,000 corrections. The results eliminated much of the chaos visible in the middle row of Fig. 3, but still the region of $D_{\text{Wit}} > 0$ is smaller than as presented in Ref.¹⁷ (see Fig. 6).

Volumentry of bound entanglement in the simplex

In each case Hiesmayr gave a detailed estimate of the relative volume of bound entangled states. In this paper we rather avoid it due to substantial differences in methodology. We do not perform a massive survey of states, but

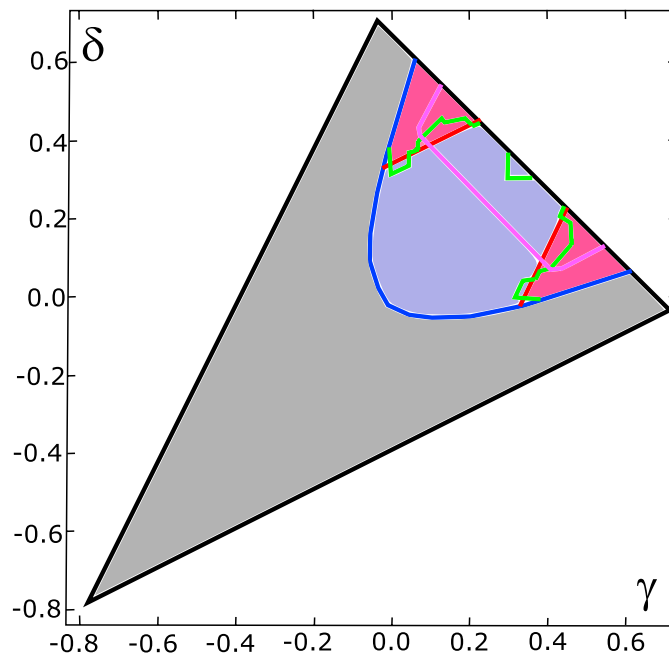


Figure 4. Classification of Family B_3 according to Ref.¹⁷. The color coding is as follows: gray: free entangled states, red: bound entangled states confirmed by linear witnesses, green and magenta lines: boundaries of the set of PPT entangled states as suggested by machine learning, with “nearest neighbours” and “random foresting”, respectively.

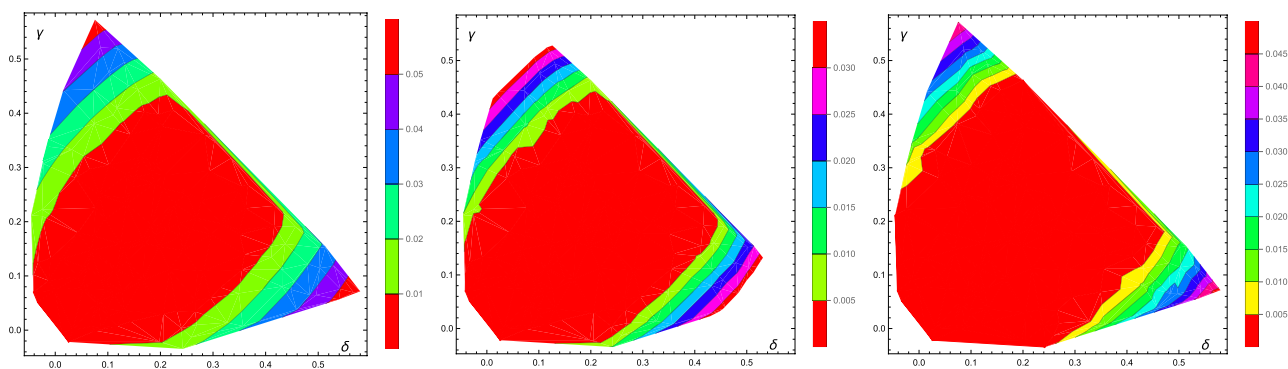


Figure 5. Interpolated plots of D_{Last} (left), D_{Est} (center), and D_{Wit} (right) for PPT states of Family B_3 .

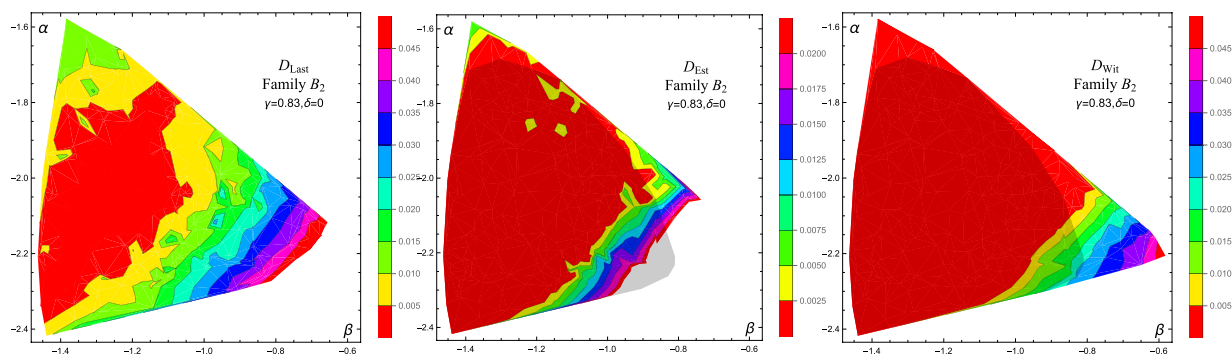


Figure 6. Interpolated plots of D_{Last} (left), D_{Est} (center), and D_{Wit} (right) for PPT states of Family B_2 with up to 40,000 corrections for selected states.

take a small sample and interpolate the results. Additionally, while the algorithm is capable of precisely estimating the distance for highly entangled states and deeply separable states, it leaves many boundary cases undecided. Moreover, we use three different estimators, each dependent on how far we go in the endless sequence of corrections. These arguments thus draw the relative volumes somewhat arbitrary. The only case where we decided to investigate this issue was the full simplex parameterized by

$$\rho = \sum_{(j,k) \neq (2,2)} p_{jk} |\psi_{jk}\rangle \langle \psi_{jk}| + \left(1 - \sum_{(j,k) \neq (2,2)} p_{jk}\right) |\psi_{22}\rangle \langle \psi_{22}|. \quad (14)$$

With probabilities $\{p_{jk}\}_{(j,k) \neq (2,2)}$ drawn at random uniformly, we generated 1000 PPT states, which took the total of 2456 physical states. This gives the ratio of 0.407 of states being PPT. We run the algorithm up to 30,000 corrections for each state and found that D_{Est} was larger than 0 for 137 states, whereas $D_{\text{Wit}} > 0$ was found in 45 cases. We have also checked the following parameterization including white noise,

$$\rho = \sum_{j,k=0}^2 a_{jk} |\psi_{jk}\rangle \langle \psi_{jk}| + \left(1 - \sum_{j,k=0}^2 a_{jk}\right) \frac{\mathbb{1}}{9}, \quad (15)$$

where each $a_{jk} \in [-1/8, 1]$ was drawn randomly with a uniform distribution. Generating 1000 PPT states took 2398 physical states, which translates into 0.417 states being PPT. Again, we have reconstructed CSSs up to 30,000 corrections. As a result, we found 139 cases of $D_{\text{Est}} > 0$ and 45 cases of $D_{\text{Wit}} > 0$.

Dynamics of D_{Est}

We also present the dynamics of D_{Est} in function of the number of corrections. Figure 7 depicts this quantity for three arbitrarily chosen states from Family B and three from the closeup of Family A (Fig. 2). The only criterion was that D_{Est} is larger than 0. While it is difficult to characterize this behavior in general, one can conclude that for many states D_{Est} stabilizes after sufficiently many corrections. This again highlights the relevance of this quantity as an entanglement estimator.

Conclusions

Until recently, even a rough classification of quantum states as separable or entangled had been a very demanding challenge, close to impossible. The Gilbert algorithm does not give a definite and final solution to this problem, but it can provide useful insight. First, it is able to provide incredibly precise approximations of some states, strongly hinting them as separable. On the other hand, it provides entanglement witnesses, directly certifying non-separability. This leaves few ambiguous cases of very weakly entangled states and those, for which subsequent corrections require particularly many trial states. This was the case of Family B_2 . In this contribution we have demonstrated that a strictly statistical interpretation of the result utilizing D_{Est} can also give a reasonable

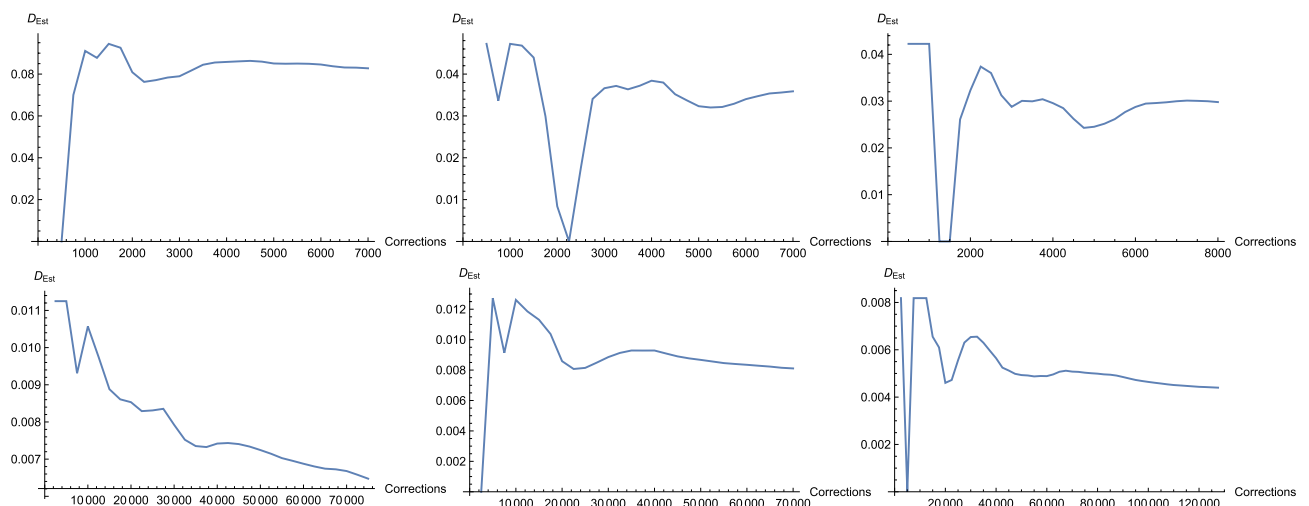


Figure 7. Dynamics of D_{Est} in function of the number of corrections for three arbitrarily selected states from Family A (top) and B (bottom).

approximation of a set of separable states. In at least one case we have certified entanglement where other combined analytical, numerical, and machine learning-based techniques have failed.

Let us stress the low hardware requirements of the algorithm. A typical computation time for a single state with up to 10,000 corrections was around 20 min on an Intel Core i9-11900K processor (running sixteen single-core instances) and all instances together utilized far less than 1 GB of RAM at any time. It is thus both computationally and resource-wise efficient.

The presented technique of “entanglement cartography” can be universally applied to identify or estimate the boundary between separable and entangled states, regardless of the dimension, the number of subsystems, or a type of quantum correlations in question. For example, it can find a variety of applications in solid state models. Importantly, the algorithm has not been fed with any information other than the input state. It is irrelevant if the state has free or bound entanglement. The technique could be combined with machine learning and interpolation techniques, but it can also generate useful results on its own. In contrast to FREE/BOUND/SEP categorization, it provides a qualitative information about entanglement. While new bound entangled states can be easily detected, the question is if their non-classicality can be meaningful in an experimental realization.

Data availability

The source code is available at <https://www.github.com/wiesnim9/CSSFinder>. The data are available from the Author upon a reasonable request at marcin.wiesniak@ug.edu.pl.

Received: 12 September 2023; Accepted: 31 October 2023

Published online: 09 November 2023

References

- Einstein, A., Podolsky, B. & Rosen, N. Can quantum-mechanical description of physical reality be considered complete?. *Phys. Rev.* **47**, 777 (1935).
- Vedral, V. & Kashefi, E. Uniqueness of the entanglement measure for bipartite pure states and thermodynamics. *Phys. Rev. Lett.* **89**, 037903 (2002).
- Peres, A. Separability criterion for density matrices. *Phys. Rev. Lett.* **77**, 1413 (1996).
- Horodecki, M., Horodecki, P. & Horodecki, R. Separability of n-particle mixed states: Necessary and sufficient conditions in terms of linear maps. *Phys. Lett. A* **283**, 1–7 (2001).
- Horodecki, P. Separability criterion and inseparable mixed states with positive partial transposition. *Phys. Lett. A* **232**, 333–339 (1997).
- Bennett, C. H. *et al.* Purification of noisy entanglement and faithful teleportation via noisy channels. *Phys. Rev. Lett.* **76**, 722 (1996).
- Jamiołkowski, A. Linear transformations which preserve trace and positive semidefiniteness of operators. *Rep. Math. Phys.* **3**, 275–278 (1972).
- Choi, M.-D. Completely positive linear maps on complex matrices. *Linear Algebra Appl.* **10**, 285–290 (1975).
- Bennett, C. H., DiVincenzo, D. P., Smolin, J. A. & Wootters, W. K. Mixed-state entanglement and quantum error correction. *Phys. Rev. A* **54**, 3824 (1996).
- Hayden, P. M., Horodecki, M. & Terhal, B. M. The asymptotic entanglement cost of preparing a quantum state. *J. Phys. A: Math. Gener.* **34**, 6891 (2001).
- Vedral, V., Plenio, M. B., Rippin, M. A. & Knight, P. L. Quantifying entanglement. *Phys. Rev. Lett.* **78**, 2275 (1997).
- Lee, S., Chi, D. P., Oh, S. D. & Kim, J. Convex-roof extended negativity as an entanglement measure for bipartite quantum systems. *Phys. Rev. A* **68**, 062304062304 (2003).
- Wang, B. Learning to detect entanglement. [arXiv:1709.03617](https://arxiv.org/abs/1709.03617) (2017).
- Gray, J., Banchi, L., Bayat, A. & Bose, S. Machine-learning-assisted many-body entanglement measurement. *Phys. Rev. Lett.* **121**, 150503 (2018).
- Chen, Y., Pan, Y., Zhang, G. & Cheng, S. Detecting quantum entanglement with unsupervised learning. *Quant. Sci. Technol.* **7**, 015005 (2021).
- Harney, C., Paternostro, M. & Pirandola, S. Mixed state entanglement classification using artificial neural networks. *N. J. Phys.* **23**, 063033 (2021).
- Hiesmayr, B. C. Free versus bound entanglement, a np-hard problem tackled by machine learning. *Sci. Rep.* **11**, 19739 (2021).
- Girardin, A., Brunner, N. & Kriváček, T. Building separable approximations for quantum states via neural networks. *Phys. Rev. Res.* **4**, 023238 (2022).
- Roik, J., Bartkiewicz, K., Černoč, A. & Lemr, K. Entanglement quantification from collective measurements processed by machine learning. *Phys. Lett. A* **446**, 128270 (2022).
- Lin, X., Chen, Z. & Wei, Z. Quantifying unknown quantum entanglement via a hybrid quantum-classical machine learning framework. [arXiv:2204.11500](https://arxiv.org/abs/2204.11500) (2022).
- Scala, F., Mangini, S., Macchiavello, C., Bajoni, D. & Gerace, D. Quantum variational learning for entanglement witnessing. In *2022 International Joint Conference on Neural Networks (IJCNN)* 1–8 (IEEE, 2022).
- Vintskevich, S., Bao, N., Nomerotski, A., Stankus, P. & Grigoriev, D. Classification of four-qubit entangled states via machine learning. [arXiv:2205.11512](https://arxiv.org/abs/2205.11512) (2022).
- Pawłowski, J. & Krawczyk, M. Quantification of entanglement with siamese convolutional neural networks. [arXiv:2210.07410](https://arxiv.org/abs/2210.07410) (2022).
- Ayachi, F. E. & Baz, M. E. General classification of entanglement using machine learning. [arXiv:2210.07711](https://arxiv.org/abs/2210.07711) (2022).
- Chen, Z., Lin, X. & Wei, Z. Certifying unknown genuine multipartite entanglement by neural networks. [arXiv:2210.13837](https://arxiv.org/abs/2210.13837) (2022).
- Consiglio, M., Apollaro, T. J. & Wieśniak, M. Variational approach to the quantum separability problem. *Phys. Rev. A* **106**, 062413 (2022).
- Ohst, T.-A., Yu, X.-D., Gühne, O. & Nguyen, H. C. Certifying quantum separability with adaptive polytopes. [arXiv:2210.10054](https://arxiv.org/abs/2210.10054) (2022).
- Witte, C. & Trucks, M. A new entanglement measure induced by the hilbert-schmidt norm. *Phys. Lett. A* **257**, 14–20 (1999).
- Ozawa, M. Entanglement measures and the hilbert-schmidt distance. *Phys. Lett. A* **268**, 158–160 (2000).
- Gilbert, E. G. An iterative procedure for computing the minimum of a quadratic form on a convex set. *SIAM J. Control* **4**, 61–80 (1966).
- Shang, J. & Gühne, O. Convex optimization over classes of multiparticle entanglement. *Phys. Rev. Lett.* **120**, 050506 (2018).
- Brierley, S., Navascues, M. & Vertesi, T. Convex separation from convex optimization for large-scale problems. [arXiv:1609.05011](https://arxiv.org/abs/1609.05011) (2016).

33. Pandya, P., Sakarya, O. & Wieśniak, M. Hilbert-schmidt distance and entanglement witnessing. *Phys. Rev. A* **102**, 012409 (2020).
34. Życzkowski, K. & Sommers, H.-J. Induced measures in the space of mixed quantum states. *J. Phys. A: Math. Gener.* **34**, 7111 (2001).
35. Bertlmann, R. A., Dürstberger, K., Hiesmayr, B. C. & Krammer, P. Optimal entanglement witnesses for qubits and qutrits. *Phys. Rev. A* **72**, 052331 (2005).
36. Wieśniak, M., Pandya, P., Sakarya, O. & Woloncewicz, B. Distance between bound entangled states from unextendible product bases and separable states. *Quant. Rep.* **2**, 49–56 (2020).
37. Popp, C. & Hiesmayr, B. C. Almost complete solution for the np-hard separability problem of bell diagonal qutrits. *Sci. Rep.* **12**, 12472 (2022).
38. Baumgartner, B., Hiesmayr, B. C. & Narnhofer, H. State space for two qutrits has a phase space structure in its core. *Phys. Rev. A* **74**, 032327 (2006).
39. Baumgartner, B., Hiesmayr, B. C. & Narnhofer, H. The geometry of bipartite qutrits including bound entanglement. *Phys. Lett. A* **372**, 2190–2195 (2008).

Acknowledgements

This work is a part of NCN Grant No. 2017/26/E/ST2/01008. MW acknowledges partial support by the Foundation for Polish Science (IRAP project, ICTQT, Contract No. 2018/MAB/5, co-financed by EU within Smart Growth Operational Programme).

Author contributions

M.W. designed, conducted, and described research.

Competing interests

The author declares no competing interests.

Additional information

Correspondence and requests for materials should be addressed to M.W.

Reprints and permissions information is available at www.nature.com/reprints.

Publisher's note Springer Nature remains neutral with regard to jurisdictional claims in published maps and institutional affiliations.



Open Access This article is licensed under a Creative Commons Attribution 4.0 International License, which permits use, sharing, adaptation, distribution and reproduction in any medium or format, as long as you give appropriate credit to the original author(s) and the source, provide a link to the Creative Commons licence, and indicate if changes were made. The images or other third party material in this article are included in the article's Creative Commons licence, unless indicated otherwise in a credit line to the material. If material is not included in the article's Creative Commons licence and your intended use is not permitted by statutory regulation or exceeds the permitted use, you will need to obtain permission directly from the copyright holder. To view a copy of this licence, visit <http://creativecommons.org/licenses/by/4.0/>.

© The Author(s) 2023